Determination of Adsorption Isotherms of Hydrogen on Titanium in Sulfuric Acid Solution Using the Phase-Shift Method and Correlation Constants

Jin Y. Chun[†] **and Jang H. Chun***[,‡]

School of Chemical and Biological Engineering, Seoul National University, Seoul 151-742, Republic of Korea, and Department of Electronic Engineering, Kwangwoon University, Seoul 139-701, Republic of Korea

The phase-shift method and correlation constants, i.e., the unique electrochemical impedance spectroscopy (EIS) techniques for studying the linear relationship between the behavior ($-\varphi$ vs E) of the phase shift ($90° \geq -\varphi \geq 0°$) for the optimum intermediate frequency and that (θ vs E) of the fractional surface coverage ($0 \leq \theta \leq 1$), have been proposed and verified to determine the Langmuir, Frumkin, and Temkin adsorption isotherms of H and related electrode kinetic and thermodynamic parameters on noble metals (alloys) in aqueous solutions. On Ti in 0.5 M H_2SO_4 aqueous solution, the Frumkin and Temkin adsorption isotherms (θ vs E), equilibrium constants ($K = 8.3 \cdot 10^{-12} \exp(-6.6\theta)$ mol^{-1} for the Frumkin, and $K = 8.3 \cdot 10^{-11} \exp(-11.2\theta)$ mol^{-1} for the Temkin adsorption isotherm), interaction parameters ($g = 6.6$ for the Frumkin and $g = 11.2$ for the Temkin adsorption isotherm), rates of change of the standard free energy ($r = 16.4$ kJ·mol^{-1} for $g = 6.6$ and $r = 27.8$ kJ·mol^{-1} for $g = 11.2$) of H with θ, and standard free energies [$(63.2 \leq \Delta G_\theta^0 \leq 79.6)$ kJ·mol^{-1} for $K = 8.3 \cdot 10^{-12} \exp(-6.6\theta)$ mol^{-1} and $0 \leq \theta \leq 1$ and $(63.1 < \Delta G_\theta^0 < 79.6)$ kJ·mol^{-1} for $K = 8.3 \cdot 10^{-11} \exp(-11.2\theta)$ mol^{-1} and $0.2 < \theta < 0.8$] of H are determined using the phase-shift method and correlation constants. At $0.2 < \theta < 0.8$, the Temkin adsorption isotherm correlating with the Frumkin adsorption isotherm, and vice versa, is readily determined using the correlation constants. The two different adsorption isotherms appear to fit the same data regardless of their adsorption conditions. The phase-shift method and correlation constants are probably the most accurate, useful, and effective ways to determine the adsorption isotherms of H and related electrode kinetic and thermodynamic parameters on highly corrosion-resistant metals in aqueous solutions.

Introduction

Titanium, titanium oxides, and titanium alloys have been widely used as implant materials due to their high corrosion resistances. Also, they have been extensively studied to use hydrogen storage materials, aerospace engineering materials, electrochemical solar energy conversion materials, etc.[1−11] However, there is not much reliable information on the Langmuir, Frumkin, and Temkin adsorption isotherms of H and related electrode kinetic and thermodynamic data on titanium in aqueous solutions.

On highly corrosion-resistant metals in aqueous solutions, it is preferable to consider the Langmuir, Frumkin, and Temkin adsorption isotherms for H rather than equations of the electrode kinetics and thermodynamics for H because these adsorption isotherms are associated more directly with the atomic mechanism of H adsorption. Thus, there is a technological need for a simple, accurate, useful, and effective method to determine the Langmuir, Frumkin, and Temkin adsorption isotherms of H and related electrode kinetic and thermodynamic parameters on highly corrosion-resistant metals in aqueous solutions.

Many scientific phenomena have been interpreted by their behaviors rather than by their natures. For example, the duality of light and electrons, i.e., the wave and particle behaviors, are well-known in science and have been applied in engineering. Note that these wave and particle behaviors are not contradictory to each other but complementary to each other. The phase-shift method and correlation constants are the unique electrochemical impedance spectroscopy (EIS) techniques for studying the linear relationship between the behavior ($-\varphi$ vs E) of the phase shift ($90° \geq -\varphi \geq 0°$) for the optimum intermediate frequency and that (θ vs E) of the fractional surface coverage ($0 \leq \theta \leq 1$) on noble metals (alloys) in aqueous solutions.[12−25] The behavior (θ vs E) of the fractional surface coverage ($0 \leq \theta \leq 1$) is well-known as the Langmuir or the Frumkin adsorption isotherm. The phase-shift method and correlation constants are probably the most accurate, useful, and effective ways to determine the Langmuir, Frumkin, and Temkin adsorption isotherms of H and related electrode kinetic and thermodynamic parameters on the noble metals (alloys) in aqueous solutions.

In practice, the theoretical derivation or the numerical calculation of a single equation for $-\varphi$ vs θ as a function of potential (E) and frequency (f) is complex due to the superposition of various effects that are inevitable on the noble metals (alloys) in aqueous solutions. This is the reason why the phase-shift method and correlation constants are necessary, useful, and effective. There are good theoretical grounds for the phase-shift method and correlation constants including interfacial electrochemistry, electrode kinetics, and EIS. New ideas, theories, and techniques must be rigorously tested, especially when unique or revolutionary, but only with pure logic and objectivity and through scientific methods and procedures. However, the arguments on the phase-shift method in the comments[26,27] do not fulfill these criteria. The arguments are substantially attributed to the misunderstanding and confusion on the newly

* Author to whom correspondence should be addressed. E-mail: jhchun@kw.ac.kr. Fax: +82-2-942-5235. Tel.: +82-2-940-5116.
[†] Seoul National University.
[‡] Kwangwoon University.

10.1021/je8006327 CCC: $40.75
Published on Web 03/02/2009

defined equivalent circuit for the phase-shift method, the simplified equivalent circuit for the optimum intermediate frequency response, the linear relationship between $-\varphi$ vs E and θ vs E for the optimum intermediate frequency, etc. These rebuttals are clearly explained, stated, and summarized in the responses.[28,29] The whole procedure of the phase-shift method and correlation constants for determining the adsorption isotherms of hydrogen and hydroxide and related electrode kinetic and thermodynamic parameters is described elsewhere.[23]

In this paper, we represent the Frumkin and Temkin adsorption isotherms of H and related electrode kinetic and thermodynamic parameters on Ti in 0.5 M H_2SO_4 aqueous solution using the phase-shift method and correlation constants. It appears that the phase-shift method and correlation constants are also useful and effective for determining the adsorption isotherms of H and related electrode kinetic and thermodynamic parameters on highly corrosion-resistant metals in aqueous solutions.

Experimental Section

Preparations. Taking into account the H^+ concentration and effects of the diffuse double layer and pH,[30] an acidic aqueous solution was prepared from H_2SO_4 (Sigma-Aldrich, reagent grade) with purified water (resistivity: > 18 MΩ·cm) obtained from a Millipore system. The 0.5 M H_2SO_4 aqueous solution (pH 0.33) was deaerated with 99.999 % purified nitrogen gas for 20 min before the experiments.

A standard three-electrode configuration was employed using a saturated calomel electrode (SCE) reference electrode and a titanium rod (Johnson Matthey, purity: 99.99 %, 3.175 mm diameter, estimated area: ca. 2.17 cm^2) working electrode. The Ti rod was polished to a mirror finish with 0.05 μm Al_2O_3 powders, ultrasonically cleaned in the purified water, and finally rinsed with acetone. A platinum wire (Johnson Matthey, purity: 99.95 %, 1.5 mm diameter) was used as the counter electrode.

Measurements. A cyclic voltammetry (CV) technique was used to achieve the steady state on Ti in 0.5 M H_2SO_4 aqueous solution. The CV experiments were conducted for 50 cycles, a scan rate of 50 mV·s^{-1}, and a scan potential of (0 to −1.0) V vs SCE. After the CV experiments, an EIS technique was used to study the relation between the phase-shift profile ($-\varphi$ vs E) for the optimum intermediate frequency and the corresponding surface-coverage profile (θ vs E), i.e., the Langmuir, the Frumkin, or the Temkin adsorption isotherm. The EIS experiments were conducted at a scan frequency of (10^4 to 0.1) Hz, a single sine wave, an ac amplitude of 5 mV, and a dc potential of (0 to −1.1) V vs SCE for the H adsorption. Taking into account the concentration and temperature of 0.5 M H_2SO_4 aqueous solution[11] and the corrosion potential of Ti in 0.5 M H_2SO_4 aqueous solution,[31] the cathodic dissolution of Ti was not considered.

The CV experiments were performed using an EG & G PAR model 273A potentiostat controlled with the PAR model 270 software package. The EIS experiments were performed using the same apparatus in conjunction with a Schlumberger SI 1255 HF frequency response analyzer controlled with the PAR model 398 software package. To obtain comparable and reproducible results, all measurements were carried out using the same preparations, procedures, and conditions at room temperature. The international sign convention is used; i.e., cathodic currents and lagged phase shifts or angles are taken as negative. To clarify the hydrogen adsorption in the different aqueous solutions, all potentials are given in the reversible hydrogen electrode (RHE) scale. The Gaussian and adsorption isotherm analyses were carried out using the Excel and Origin software packages.

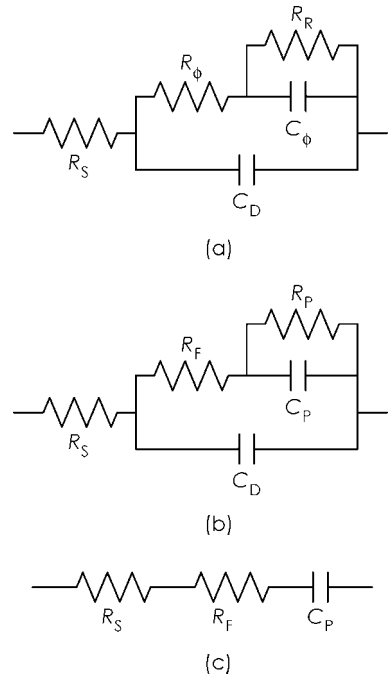

Figure 1. (a) Numerically proposed equivalent circuit for an adsorption in refs 32 and 33, (b) experimentally proposed equivalent circuit for the phase-shift method, and (c) simplified equivalent circuit for the optimum intermediate frequency response. Equivalent circuit elements shown in Figure 1b are defined in this work.

Results and Discussion

Basic Concept and Description on the Phase-Shift Method. The equivalent circuit for the H adsorption on Ti in 0.5 M H_2SO_4 aqueous solution, i.e., at the Ti/0.5 M H_2SO_4 aqueous solution interface, can be expressed as shown in Figure 1a.[32−35] In Figure 1a, R_S is the aqueous solution resistance; R_ϕ is the faradaic resistance for the H adsorption; R_R is the faradaic resistance for the recombination reaction; C_ϕ is the pseudocapacitance for the H adsorption; and C_D is the double-layer capacitance. Note that R_ϕ depends on C_ϕ. Both R_ϕ and C_ϕ are not constant but dependent on potential (E) and fractional surface coverage (θ) and cannot be measured due to the superposition of various effects at the interface.

In interfacial electrochemistry, electrode kinetics, and EIS,[32−41] a unique feature of R_ϕ and C_ϕ attaining maximum values at $\theta = 0.5$, decreasing symmetrically with E at other values of θ, approaching minimum values at $\theta \approx 0$ and 1, and attaining minimum values at $\theta = 0$ and 1 is well-known. However, the linear relationship between $-\varphi$ vs E and θ vs E due to the unique feature and combination of R_ϕ and C_ϕ vs E for the optimum intermediate frequency has never been studied in the conventional methods. At the optimum intermediate frequency, the normalized change rate of $-\varphi$ vs E, i.e., $\Delta(-\varphi)/\Delta E$, corresponds to that of θ vs E, i.e., $\Delta\theta/\Delta E$, and vice versa. Both $\Delta(-\varphi)/\Delta E$ and $\Delta\theta/\Delta E$ are maximized at $\theta \approx 0.5$, decrease symmetrically with E at other values of θ, and are minimized at $\theta \approx 0$ and 1. This linear relationship between $-\varphi$ vs E and θ vs E for the optimum intermediate frequency is the basic concept of the phase-shift method and has been experimentally and consistently verified.[12−25] Note that this is the unique feature and combination of R_ϕ and C_ϕ vs E for the optimum intermediate frequency, i.e., the phase-shift profile ($-\varphi$ vs E) of the phase shift ($90° \geq -\varphi \geq 0°$) for the optimum intermediate frequency. Also, this is a unique feature of the Langmuir or the Frumkin adsorption isotherm, i.e., the surface-coverage profile (θ vs E)

of θ ($0 \leq \theta \leq 1$). The numerical derivation of C_ϕ from the Langmuir or the Frumkin adsorption isotherm is described elsewhere.[32,33] In electrosorption, θ is a function of E.[36,37] The Langmuir and Frumkin adsorption isotherms describe the dependence of θ on E.[38−41] However, as stated above, both R_ϕ and C_ϕ cannot be measured due to the superposition of various effects. This is the reason why the phase-shift method is unique, useful, and effective. These aspects are discussed in more detail later.

Taking into account the superposition of various effects (relaxation time effects, real surface area problems, surface absorption and diffusion processes, inhomogeneous and lateral interaction effects, specific adsorption effects, etc.) that are inevitable under the EIS measurements, we define the equivalent circuit elements shown in Figure 1b. R_S is the aqueous solution resistance; R_F is the real resistance due to the faradaic resistance (R_ϕ) and superposition of various effects; R_P is the real resistance due to the faradaic resistance (R_R) and superposition of various effects; C_P is the real capacitance due to the pseudocapacitance (C_ϕ) and superposition of various effects; and C_D is the double-layer capacitance. Note that both R_F and C_P are not constant but dependent on E and θ and can be measured.

The frequency response of the equivalent circuit for all frequencies shown in Figure 1b is essential for verifying the unique feature and combination of R_ϕ and C_ϕ vs E for the optimum intermediate frequency, i.e., the linear relationship between $-\varphi$ vs E and θ vs E for the optimum intermediate frequency. At very low frequencies, the equivalent circuit for all frequencies shown in Figure 1b can be expressed as a series circuit of R_S, R_F, and R_P. At very high frequencies, the equivalent circuit for all frequencies shown in Figure 1b can be expressed as a series circuit of R_S and C_D. At the optimum intermediate frequency and for a wide range of θ, the equivalent circuit for all frequencies shown in Figure 1b can be simplified as the series circuit of R_S, R_F, and C_P shown in Figure 1c. However, note that the simplified equivalent circuit shown in Figure 1c is not for the change of the H adsorption itself but only the optimum intermediate frequency response.

The impedance (Z) of the simplified equivalent circuit shown in Figure 1c and the corresponding lagged phase shift ($-\varphi$) are given by

$$Z = (R_S + R_F) - j/\omega C_P \quad (1)$$

$$-\varphi = \tan^{-1}[1/\omega(R_S + R_F)C_P] \quad (2)$$

$R_F \gg R_S$ and $C_P \gg C_D$ (for a wide range of θ)

$$R_P \gg 1/\omega C_P,\ R_F \propto R_\phi, \text{ and } C_P \propto C_\phi \quad (3)$$

where j is an operator and is equal to the square root of -1, i.e., $j^2 = -1$; ω ($= 2\pi f$) is the angular frequency; f is the optimum intermediate frequency; and θ ($0 \leq \theta \leq 1$) is the fractional surface coverage of H. For a wide range of θ, the measured values of R_F and C_P are much greater than those of R_S and C_D, respectively. Therefore, $-\varphi$ described in eq 2 is substantially determined by the combination of R_F and C_P.

Figures 2a and b show the profiles of R_F vs E and C_P vs E for the optimum intermediate frequency (5.012 Hz), respectively. Figure 2a shows that R_F is smaller than R_ϕ because the left side of the real resistance profile (R_F vs E) is lower than the right side of the real resistance profile (R_F vs E). Figure 2b shows

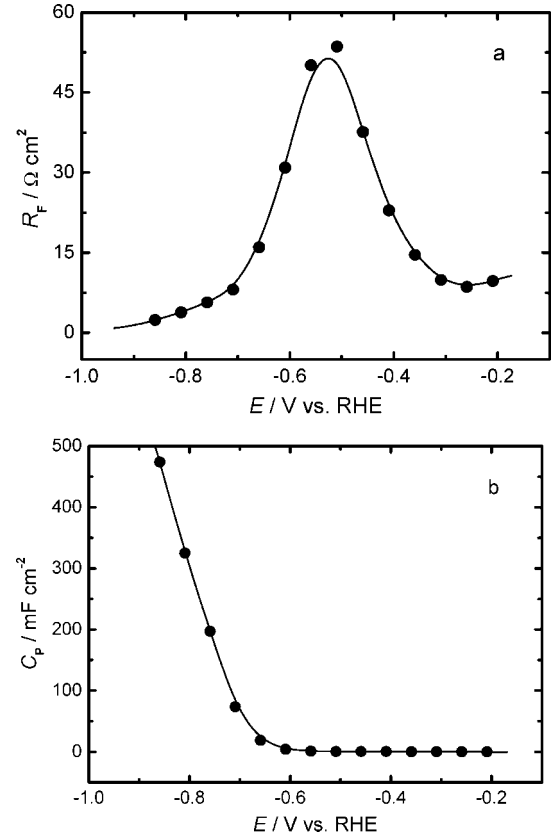

Figure 2. Profiles of the real circuit elements (R_F, C_P) vs E for the optimum intermediate frequency (5.012 Hz). RHE: reversible hydrogen electrode. ●, measured values. (a) Real resistance profile (R_F vs E) and (b) real capacitance profile (C_P vs E).

that C_P is greater than C_ϕ because the real capacitance profile (C_P vs E) increases from the right side to the left side, i.e., toward more negative potentials. This is attributed to the reciprocal property of R_F and C_P due to the superposition of various effects. The nature of R_F is inversely proportional to the concentration of charged species (H^+) due to the superposition of various effects, but the nature of C_P is proportional to the concentration of charged species (H^+) due to the superposition of various effects. However, note that the real resistance profile (R_F vs E) shown in Figure 2a has a peak. But, the real capacitance profile (C_P vs E) shown in Figure 2b has no peak. This is also attributed to the reciprocal property of R_F and C_P due to the superposition of various effects. Consequently, one can interpret that the superposition of various effects of R_F and C_P in eq 2 is canceled out or compensated together, and so the combination of R_F and C_P is equivalent to that of R_ϕ and C_ϕ.

Figure 3 compares the Nyquist impedance plots (Z_{IM} vs Z_{RE}) for different potentials (E). In this figure, Z_{IM} and Z_{RE} refer to the imaginary and real parts of the impedance (Z), respectively. The values of ω ($= 2\pi f$), which are not shown in Figure 3, increase from the outside, i.e., 0.1 Hz, to the origin of the Z_{IM} and Z_{RE} axes, i.e., 10^4 Hz. Note that Z_{IM} and Z_{RE} are not constant but dependent on E and θ, i.e., the H adsorption. Figures 3f−i show that the intermediate frequency loops appear at negatively high potentials. It seems to be related to the cathodic H_2 evolution and/or the cathodic dissolution of Ti.[11,31,33−35]

Figure 4 compares the phase-shift curves ($-\varphi$ vs $\log f$) for the different potentials (E). Note that $-\varphi$ vs $\log f$ shown in Figure 4 corresponds to Z_{IM} vs Z_{RE} shown in Figure 3 and vice versa. The intermediate frequency, i.e., a vertical solid line (5.012 Hz) on $-\varphi$ vs $\log f$ shown in Figure 4, can be set as the

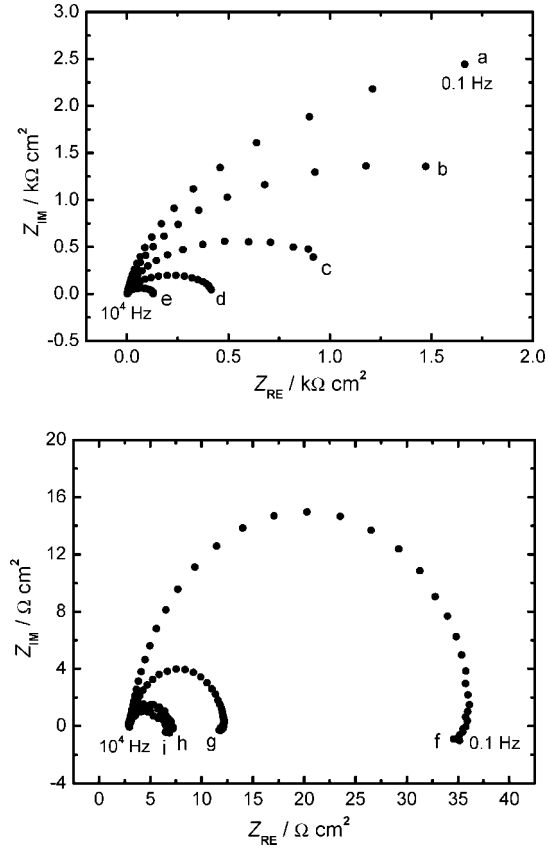

Figure 3. Comparison of the Nyquist impedance plots (Z_{IM} vs Z_{RE}) for different potentials. ●, measured values. Single sine wave; scan frequency: (10^4 to 0.1) Hz; ac amplitude: 5 mV; dc potential: (a) −0.209 V, (b) −0.259 V, (c) −0.309 V, (d) −0.409 V, (e) −0.509 V, (f) −0.609 V, (g) −0.709 V, (h) −0.809 V, and (i) −0.859 V vs RHE. All frequencies increase from the outside (0.1 Hz) to the origin of Z_{IM} and Z_{RE} axes (10^4 Hz).

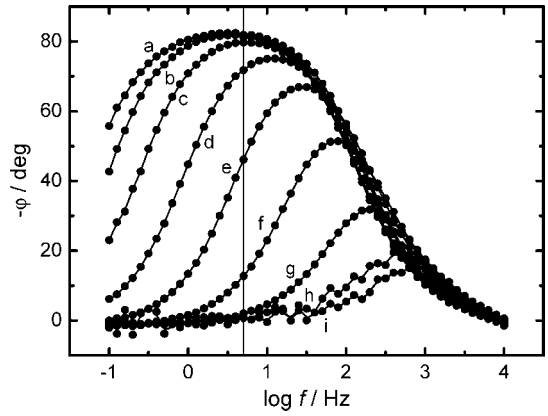

Figure 4. Comparison of the phase-shift curves ($-\varphi$ vs log f) for different potentials. ●, measured values. Vertical solid line: 5.012 Hz; single sine wave; scan frequency: (10^4 to 0.1) Hz; ac amplitude: 5 mV; dc potential: (a) −0.209 V, (b) −0.259 V, (c) −0.309 V, (d) −0.409 V, (e) −0.509 V, (f) −0.609 V, (g) −0.709 V, (h) −0.809 V, and (i) −0.859 V vs RHE.

optimum intermediate frequency for $-\varphi$ vs E and θ vs E. At the maximum lagged phase shift (81.8°) shown in Figure 4a, it appears that the H adsorption and superposition of various effects are minimized due to the low potential (−0.209 V vs RHE), i.e., $\theta \approx 0$. Note that θ is a function of E. At $\theta \approx 0$, $1/\omega C_P$ is much greater than $(R_S + R_F)$ (see Figure 3a). In eqs 1 to 3, Z is substantially determined by $1/\omega C_P$, i.e., Z_{IM}, and so $-\varphi$ has a maximum value of ≤ 90°. For a pure capacitor, $-\varphi$ is 90°. Both $\Delta(-\varphi)/\Delta E$ and $\Delta\theta/\Delta E$ are minimized due to R_ϕ and C_ϕ approaching minimum values at $\theta \approx 0$. At the minimum

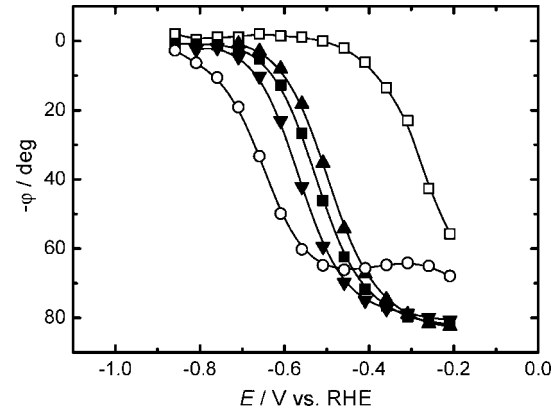

Figure 5. Comparison of the phase-shift profiles ($-\varphi$ vs E) for five different frequencies. Measured values: □, 0.1 Hz; ▲, 3.162 Hz; ■, 5.012 Hz; ▼, 10 Hz; ○, 50.12 Hz. The optimum intermediate frequency is 5.012 Hz (■).

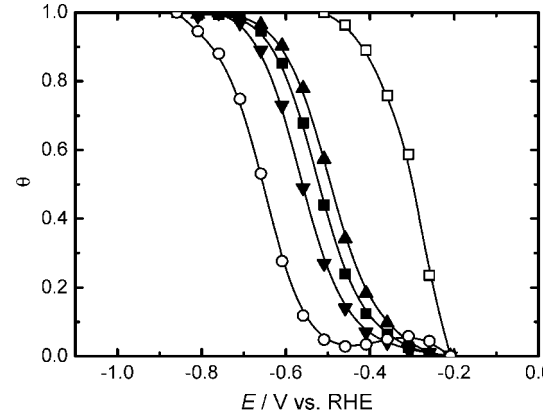

Figure 6. Comparison of the surface-coverage profiles (θ vs E) for five different frequencies. Measured values: □, 0.1 Hz; ▲, 3.162 Hz; ■, 5.012 Hz; ▼, 10 Hz; ○, 50.12 Hz. The optimum intermediate frequency is 5.012 Hz (■).

lagged phase shift (0.7°) shown in Figure 4i, it appears that the H adsorption and superposition of various effects are maximized or almost saturated due to the high potential (−0.859 V vs RHE), i.e., $\theta \approx 1$. At $\theta \approx 1$, $(R_S + R_F)$ is much greater than $1/\omega C_P$ (see Figure 3i). In eqs 1 to 3, Z is substantially determined by $(R_S + R_F)$, i.e., Z_{RE}, and so $-\varphi$ has a minimum value of ≥ 0°. For a pure resistor, $-\varphi$ is 0°. Both $\Delta(-\varphi)/\Delta E$ and $\Delta\theta/\Delta E$ are also minimized due to R_ϕ and C_ϕ approaching minimum values at $\theta \approx 1$. At the medium lagged phase shift (46.1°) shown in Figure 4e, i.e., at the intermediate potential (−0.509 V vs RHE), it appears that both $\Delta(-\varphi)/\Delta E$ and $\Delta\theta/\Delta E$ are maximized due to R_ϕ and C_ϕ approaching maximum values at $\theta \approx 0.5$. At other lagged phase shifts (79.7° to 2.0°) shown in Figures 4c, d, f, and g, i.e., at other potentials (−0.309 V, −0.409 V, −0.609 V, and −0.709 V vs RHE), it appears that both $\Delta(-\varphi)/\Delta E$ and $\Delta\theta/\Delta E$ decrease symmetrically with E due to R_ϕ and C_ϕ decreasing symmetrically with E at other values of θ.

On the basis of $-\varphi$ vs log f shown in Figure 4, the linear relationship between $-\varphi$ vs E and θ vs E for the optimum intermediate frequency,[12−25] and the unique feature of electrosorption,[36,37] the basic concept and description on the phase-shift method are summarized in Table 1. Table 1 shows the changes of $-\varphi$ vs E and θ vs E for the optimum intermediate frequency (5.012 Hz) with 50 mV increment changes in negative potential (E). These changes of $-\varphi$ vs E and θ vs E for 5.012 Hz are plotted in Figures 5 and 6, respectively. The changes of $-\varphi$ vs E and θ vs E for other frequencies (0.1 Hz, 3.162 Hz, 10 Hz, 50.12 Hz) plotted in Figures 5 and 6, respectively, are also

Table 1. Measured Values of the Phase Shift ($-\varphi$) for the Optimum Intermediate Frequency (5.012 Hz), the Estimated Fractional Surface Coverage (θ) of H, and the Normalized Change Rates ($\Delta(-\varphi)/\Delta E$, $\Delta\theta/\Delta E$)

E/V vs RHE	$-\varphi$/deg	θ ($0 \le \theta \le 1$)	$\Delta(-\varphi)$, $\Delta\theta/\Delta E$
−0.209	81.8	≈ 0	−
−0.259	81.2	0.007398	0.096178
−0.309	79.7	0.025894	0.240444
−0.359	76.6	0.064118	0.496917
−0.409	71.8	0.123305	0.769420
−0.459	62.4	0.239211	1.506782
−0.509	46.1	0.440197	2.612824
−0.559	26.7	0.679408	3.109741
−0.609	12.7	0.852035	2.244143
−0.659	5.1	0.945746	1.218249
−0.709	2.0	0.983970	0.496917
−0.759	1.1	0.995068	0.144266
−0.809	0.8	0.998767	0.048089
−0.859	0.7	≈ 1	0.016030

obtained through the same procedures summarized in Table 1. Note that θ vs E shown in Figure 6 corresponds to $-\varphi$ vs E shown in Figure 5 and vice versa.

Figure 7 shows the normalized change rates of $-\varphi$ vs E and θ vs E, i.e., $\Delta(-\varphi)/\Delta E$ and $\Delta\theta/\Delta E$, for the five different frequencies. In Figure 7, $\Delta(-\varphi)/\Delta E$ and $\Delta\theta/\Delta E$ are plotted based on $-\varphi$ vs E and θ vs E shown in Figures 5 and 6, respectively. In Figure 7c, both $\Delta(-\varphi)/\Delta E$ and $\Delta\theta/\Delta E$ are maximized at $\theta \approx 0.5$, decrease symmetrically with E at other values of θ, and are minimized at $\theta \approx 0$ and 1. The Gaussian profile shown in Figure 7c is plotted based on both $\Delta(-\varphi)/\Delta E$ and $\Delta\theta/\Delta E$ for the optimum intermediate frequency (5.012 Hz) summarized in Table 1. Similarly, the Gaussian profiles for 0.1 Hz, 3.162 Hz, 10 Hz, and 50.12 Hz shown in Figures 7a, b, d, and e, respectively, are plotted through the same procedures summarized in Table 1. Note that the Gaussian profile shown in Figure 7c is the unique feature of the Frumkin adsorption isotherm (θ vs E). Table 1 also shows that both $\Delta(-\varphi)/\Delta E$ and $\Delta\theta/\Delta E$ for the optimum intermediate frequency (5.012 Hz) are exactly the same.

Finally, one can conclude that the discussions on Z and $-\varphi$ described in eqs 1 to 3 and Table 1, the reciprocal property and compensation of R_F and C_P in eq 2, the determination of the optimum intermediate frequency for $-\varphi$ vs E and θ vs E shown in Figures 4 to 7, and the linear relationship between $-\varphi$ vs E and θ vs E for the optimum intermediate frequency are valid and correct.

Frumkin, Langmuir, and Temkin Adsorption Isotherms. The derivation and interpretation of the practical forms of the electrochemical Langmuir, Frumkin, and Temkin adsorption isotherms are described elsewhere.[38−41] The Frumkin adsorption isotherm assumes that the surface is inhomogeneous or that the lateral interaction effect is not negligible. The Frumkin adsorption isotherm (θ vs E) of H can be expressed as follows[38]

$$[\theta/(1-\theta)]\exp(g\theta) = K_o C_{H^+}[\exp(-EF/RT)] \quad (4)$$

$$g = r/RT \quad (5)$$

$$K = K_o \exp(-g\theta) \quad (6)$$

where θ ($0 \le \theta \le 1$) is the fractional surface coverage of H; g is the interaction parameter for the Frumkin adsorption isotherm; K_o is the equilibrium constant for H at $g = 0$; C_{H^+} is the H^+ concentration in the bulk solution; E is the negative potential; F is Faraday's constant; R is the gas constant; T is the absolute temperature; r is the rate of change of the standard free energy of H with θ; and K is the equilibrium constant for H. The dimension of K is described elsewhere.[42] Note that $g = 0$ in eqs 4 to 6 implies the Langmuir adsorption isotherm. For the Langmuir adsorption isotherm, the inhomogeneous and lateral interaction effects on the H adsorption are negligible.

For the H adsorption on Ti in 0.5 M H_2SO_4 aqueous solution, the numerically calculated Frumkin adsorption isotherms using eq 4 are shown in Figure 8. Figures 8a, b, and c show the three numerically calculated Frumkin adsorption isotherms corresponding to $g = 0$, 6.6, and 13.2 for $K_o = 8.3 \cdot 10^{-12}$ mol^{-1}, respectively. Note that the Frumkin adsorption isotherm (θ vs E) shown in Figure 8b is linearly related to the phase-shift profile ($-\varphi$ vs E) for the optimum intermediate frequency (5.012 Hz) shown in Figure 5. In Figure 8b, one infers that $K = 8.3 \cdot 10^{-12} \exp(-6.6\theta)$ mol^{-1} for the Frumkin adsorption isotherm is correctly applicable to the H adsorption. Using eq 5, r is 16.4 kJ·mol^{-1}. In Figure 8a, $g = 0$ for $K_o = 8.3 \cdot 10^{-12}$ mol^{-1} implies the Langmuir adsorption isotherm, i.e., $K = 8.3 \cdot 10^{-12}$ mol^{-1}. Note that the value of K_o for Ti is $\sim 10^5$ to 10^8 times less than that for the noble metals (alloys).[12,13,15−25] Regarding the H adsorption, Ti is a highly corrosion-resistant metal in aqueous solutions but is not a suitable metal itself for the cathodic H_2 evolution in aqueous solutions.

At intermediate values of θ, i.e., $0.2 < \theta < 0.8$, the pre-exponential term, $[\theta/(1-\theta)]$, varies little with θ compared to the variation of the exponential term, $\exp(g\theta)$ (see eq 4). Under the approximate conditions, the Temkin adsorption isotherm can be simply derived from the Frumkin adsorption isotherm. The Temkin adsorption isotherm (θ vs E) of H can be expressed as follows[38]

$$\exp(g\theta) = K_o C_{H^+}[\exp(-EF/RT)] \quad (7)$$

Figure 9 shows the determination of the Temkin adsorption isotherm correlating with the Frumkin adsorption isotherm shown in Figure 8b. Figures 9a, b, and c show the three numerically calculated Temkin adsorption isotherms corresponding to $g = 0$, 11.2, and 22.4 for $K_o = 8.3 \cdot 10^{-11}$ mol^{-1}, respectively. In Figure 9b, the numerically calculated Temkin adsorption isotherm using eq 7 is $K = 8.3 \cdot 10^{-11} \exp(-11.2\theta)$ mol^{-1}. Using eq 5, r is 27.8 kJ·mol^{-1}. Note that the Temkin adsorption isotherm shown in Figure 9b is only valid and effective at $0.2 < \theta < 0.8$.

Correlation Constants between the Adsorption Isotherms. As previously described, the Langmuir, Frumkin, and Temkin adsorption conditions are different from each other. Only one adsorption isotherm is determined based on the relevant experimental results (see Figure 8). However, as shown in Figure 9, the two different adsorption isotherms, i.e., the Temkin and Frumkin adsorption isotherms, appear to fit the same data at $0.2 < \theta < 0.8$. It has been experimentally and consistently verified using the phase-shift method and correlation constants.[20,22−25] Note that these aspects are not contradictory to each other but complementary to each other.

At $0.2 < \theta < 0.8$, the Langmuir adsorption isotherms are always parallel to each other.[15,18−20,24,38−41] This implies that the slopes of the Langmuir adsorption isotherms are all the same at this region. In other words, the value of g for the Temkin adsorption isotherm correlating with the Langmuir adsorption isotherm is the same. The value of g for the Temkin adsorption isotherm is ca. 4.6 greater than that for the correlating Langmuir adsorption isotherm.[20,22−25] Note that the Langmuir and Temkin

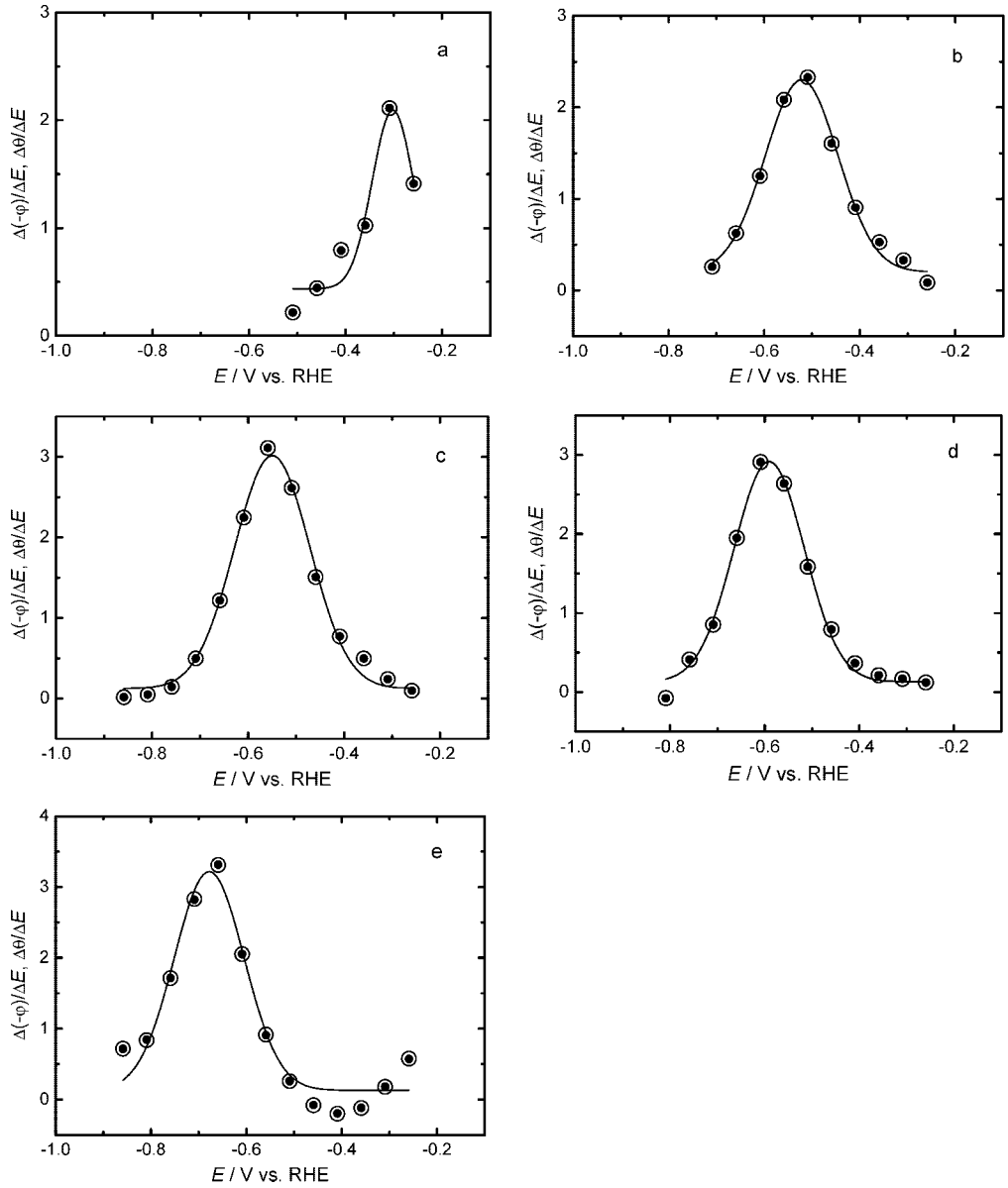

Figure 7. Comparison of the normalized change rates of $-\varphi$ vs E and θ vs E, $\Delta(-\varphi)/\Delta E$ and $\Delta\theta/\Delta E$, for five different frequencies. −, Fitted Gaussian profiles: ○, $\Delta(-\varphi)/\Delta E$; ●, $\Delta\theta/\Delta E$. (a) 0.1 Hz, (b) 3.162 Hz, (c) 5.012 Hz, (d) 10 Hz, and (e) 50.12 Hz. The optimum intermediate frequency is 5.012 Hz.

adsorption isotherms are correlated with each other even though their adsorption conditions are different. Similarly, one can interpret that the value of g for the Temkin adsorption isotherm is ca. 4.6 greater than that for the correlating Frumkin adsorption isotherm (see Figure 9) because the value of g for the Frumkin adsorption isotherm is determined referred to that for the Langmuir adsorption isotherm, i.e., $g = 0$ (see Figure 8).[14,22−25,38−41] However, for the reliable correlation between the Temkin and Langmuir or Frumkin adsorption isotherms, a wide range of K is more reasonable. In other words, the value of g should be determined at $\theta \approx 0.2$ and 0.8. In addition, one can confirm that the value of K_o for the Temkin adsorption isotherm is ca. 10 times greater than that (K or K_o) for the correlating Langmuir or Frumkin adsorption isotherm (see Figure 9).[20,22−25]

Finally, one can conclude that these numbers, ca. 10 times and 4.6, can be taken as correlation constants between the Temkin and Langmuir or Frumkin adsorption isotherms. The Temkin adsorption isotherm correlating with the Langmuir or the Frumkin adsorption isotherm, and vice versa, is readily determined using the correlation constants.

Standard Free Energy of Adsorption. The standard free energy of H is given by the difference between the standard molar Gibbs free energy of H and that of a number of water molecules on the adsorption sites of the electrode surface. Under the Frumkin adsorption conditions, the relation between the equilibrium constant (K) and the standard free energy (ΔG_θ^0) of H is given as follows[37,38]

$$2.3RT \log K = -\Delta G_\theta^{\,0} \tag{8}$$

On Ti in 0.5 M H_2SO_4 aqueous solution, using eqs 6 and 8, ΔG_θ^0 of H is ($63.2 \le \Delta G_\theta^0 \le 79.6$) kJ·mol^{-1} for ($8.3\cdot10^{-12} \ge K \ge 1.1\cdot10^{-14}$) mol^{-1}, i.e., $K = 8.3\cdot10^{-12}\exp(-6.6\theta)$ mol^{-1} and $0 \le \theta \le 1$. The standard free energies (ΔG_θ^0) of H and the equilibrium constants (K) for the Frumkin and Temkin adsorption isotherms (θ vs E) of H are summarized in Table 2.

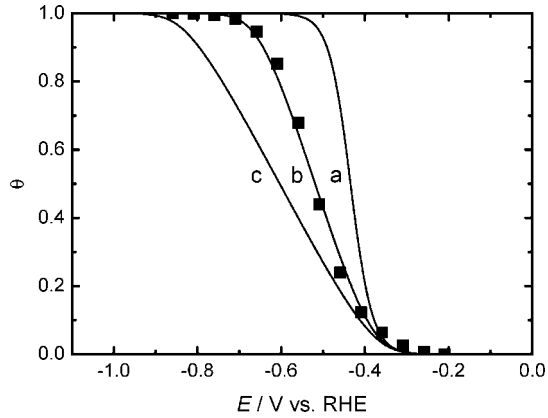

Figure 8. Comparison of the experimental and fitted data for the Frumkin adsorption isotherms (θ vs E). ■, Experimental data. −, Calculated values using eq 4. (a) $g = 0$, (b) $g = 6.6$, and (c) $g = 13.2$ for $K_o = 8.3 \cdot 10^{-12}$ mol^{-1}. Using eqs 4 to 6: (a) $g = 0$ for $K_o = 8.3 \cdot 10^{-12}$ mol^{-1} is the Langmuir adsorption isotherm, i.e., $K = 8.3 \cdot 10^{-12}$ mol^{-1}.

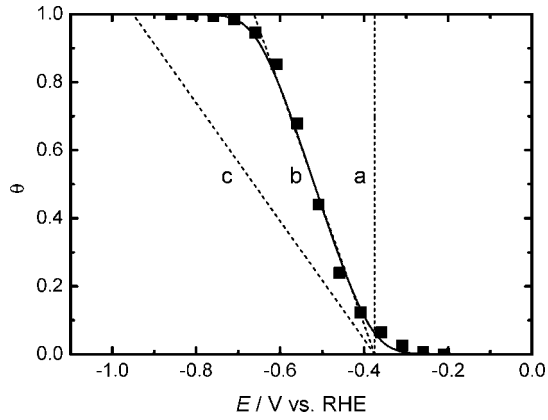

Figure 9. Comparison of the experimentally determined Frumkin adsorption isotherm and three fitted Temkin adsorption isotherms (θ vs E). ■, Experimental data. −, Calculated values using eq 4 (Frumkin adsorption isotherm). - - - -, Calculated values using eq 7 (Temkin adsorption isotherm). (a) $g = 0$, (b) $g = 11.2$, and (c) $g = 22.4$ for $K_o = 8.3 \cdot 10^{-11}$ mol^{-1}. The Temkin adsorption isotherm, (b) $g = 11.2$ for $K_o = 8.3 \cdot 10^{-11}$ mol^{-1}, i.e., $K = 8.3 \cdot 10^{-11} \exp(-11.2\theta)$ mol^{-1}, is only valid and effective at $0.2 < \theta < 0.8$.

Table 2. Comparison of the Standard Free Energies (ΔG_θ^0) of H and the Equilibrium Constants (K) for the Frumkin and Temkin Adsorption Isotherms (θ vs E) of H

adsorption isotherm	ΔG_θ^0/kJ·mol^{-1}	K/mol^{-1}	θ
Frumkin[a]	$63.2 \le \Delta G_\theta^0 \le 79.6$	$8.3 \cdot 10^{-12} \ge K \ge 1.1 \cdot 10^{-14}$	$0 \le \theta \le 1$
Temkin[b]	$63.1 < \Delta G_\theta^0 < 79.6$	$8.8 \cdot 10^{-12} > K > 1.1 \cdot 10^{-14}$	$0.2 < \theta < 0.8$

[a] $K = 8.3 \cdot 10^{-12} \exp(-6.6\theta)$ mol^{-1} (see Figure 8b). [b] $K = 8.3 \cdot 10^{-11} \exp(-11.2\theta)$ mol^{-1} (see Figure 9b). The Temkin adsorption isotherm is only valid and effective at $0.2 < \theta < 0.8$.

Conclusions

The phase-shift method and correlation constants, i.e., the unique electrochemical impedance spectroscopy (EIS) techniques for studying the linear relationship between the behavior ($-\varphi$ vs E) of the phase shift ($90° \ge -\varphi \ge 0°$) for the optimum intermediate frequency and that (θ vs E) of the fractional surface coverage ($0 \le \theta \le 1$), have been proposed and verified to determine the Langmuir, Frumkin, and Temkin adsorption isotherms of H and related electrode kinetic and thermodynamic parameters on the noble metals (alloys) in aqueous solutions.

On Ti in 0.5 M H_2SO_4 aqueous solution, the Frumkin and Temkin adsorption isotherms (θ vs E), equilibrium constants ($K = 8.3 \cdot 10^{-12} \exp(-6.6\theta)$ mol^{-1} for the Frumkin and $K = 8.3 \cdot 10^{-11} \exp(-11.2\theta)$ mol^{-1} for the Temkin adsorption isotherm), interaction parameters ($g = 6.6$ for the Frumkin and $g = 11.2$ for the Temkin adsorption isotherm), rates of change of the standard free energy ($r = 16.4$ kJ·mol^{-1} for $g = 6.6$ and $r = 27.8$ kJ·mol^{-1} for $g = 11.2$) of H with θ, and standard free energies ($(63.2 \le \Delta G_\theta^0 \le 79.6)$ kJ·mol^{-1} for $K = 8.3 \cdot 10^{-12} \exp(-6.6\theta)$ mol^{-1} and $0 \le \theta \le 1$ and $(63.1 < \Delta G_\theta^0 < 79.6)$ kJ·mol^{-1} for $K = 8.3 \cdot 10^{-11} \exp(-11.2\theta)$ mol^{-1} and $0.2 < \theta < 0.8$) of H are determined using the phase-shift method and correlation constants.

At $0.2 < \theta < 0.8$, the Temkin adsorption isotherm, $K = 8.3 \cdot 10^{-11} \exp(-11.2\theta)$ mol^{-1}, correlating with the Frumkin adsorption isotherm, $K = 8.3 \cdot 10^{-12} \exp(-6.6\theta)$ mol^{-1}, and vice versa, is readily determined using the correlation constants. The two different adsorption isotherms appear to fit the same data regardless of their adsorption conditions.

The phase-shift method and correlation constants are probably the most accurate, useful, and effective ways to determine the adsorption isotherms of H and related electrode kinetic and thermodynamic parameters on highly corrosion-resistant metals in aqueous solutions.

Note Added after ASAP Publication: This paper was published ASAP on March 2, 2009. There was a change to the notation in the text above equation 7. The revised paper was reposted on March 18, 2009.

Literature Cited

(1) Luan, B.; Zhao, H.; Liu, H. K.; Dou, S. X. On the discharging process of titanium-based hydrogen storage alloy electrode via a.c. impedance analysis. *J. Power Sources* **1996**, *62*, 75–79.
(2) Tun, Z.; Noel, J. J.; Shoesmith, D. W. Electrochemical modifications on the surface of a Ti film. *Physica B* **1998**, *241−243*, 1107–1109.
(3) Bonilla, S. H.; Zinola, C. F. Changes in the voltammetric response of titanium electrodes caused by potential programs and illumination. *Electrochim. Acta* **1998**, *43*, 423–426.
(4) Ohtsuka, T.; Otsuki, T. Effect of ultra-violet light irradiation on anodic oxide films on titanium in sulfuric acid solution. *J. Electroanal. Chem.* **1999**, *473*, 272–278.
(5) Senkov, O. N.; Froes, F. H. Thermohydrogen processing of titanium alloys. *Int. J. Hydrogen Energy* **1999**, *24*, 565–576.
(6) Blackwood, D. J. Influence of the space-charge region on electrochemical impedance measurements on passive oxide films on titanium. *Electrochim. Acta* **2000**, *46*, 563–569.
(7) Poznyak, S. K.; Talapin, D. V.; Kulak, A. I. Electrochemical oxidation of titanium by pulsed discharge in electrolyte. *J. Electroanal. Chem.* **2005**, *579*, 299–310.
(8) Takasaki, A.; Kelton, K. F. Hydrogen storage in Ti-based quasicrystal powders produced by mechanical alloying. *Int. J. Hydrogen Energy* **2006**, *31*, 183–190.
(9) Nowotny, J.; Bak, T.; Nowotny, M. K.; Sheppard, L. R. Titanium dioxide for solar-hydrogen: I. Functional properties. *Int. J. Hydrogen Energy* **2007**, *32*, 2609–2629.
(10) Ferri, T.; Gozzi, D.; Latini, A. Hydrogen evolution reaction (HER) at thin film and bulk TiC electrodes. *Int. J. Hydrogen Energy* **2007**, *32*, 4692–4701.
(11) Azumi, K.; Nakajima, M.; Okamoto, K.; Seo, M. Dissolution of Ti wires in sulphuric acid and hydrochloric acid solutions. *Corros. Sci.* **2007**, *49*, 469–480.
(12) Chun, J. H.; Ra, K. H. The phase-shift method for the Frumkin adsorption isotherms at the Pd/H_2SO_4 and KOH solution interfaces. *J. Electrochem. Soc.* **1998**, *145*, 3794–3798.
(13) Chun, J. H.; Ra, K. H.; Kim, N. Y. The Langmuir adsorption isotherms of electroadsorbed hydrogens for the cathodic hydrogen evolution reactions at the Pt(100)/H_2SO_4 and LiOH aqueous electrolyte interfaces. *Int. J. Hydrogen Energy* **2001**, *26*, 941–948.
(14) Chun, J. H.; Ra, K. H.; Kim, N. Y. Qualitative analysis of the Frumkin adsorption isotherm of the over-potentially deposited hydrogen at the poly-Ni/KOH aqueous electrolyte interface using the phase-shift method. *J. Electrochem. Soc.* **2002**, *149*, E325–330.
(15) Chun, J. H.; Ra, K. H.; Kim, N. Y. Langmuir adsorption isotherms of over-potentially deposited hydrogen at poly-Au and Rh/H_2SO_4 aqueous electrolyte interfaces: Qualitative analysis using the phase-shift method. *J. Electrochem. Soc.* **2003**, *150*, E207–217.

(16) Chun, J. H.; Jeon, S. K. Determination of the equilibrium constant and standard free energy of the over-potentially deposited hydrogen for the cathodic H_2 evolution reaction at the Pt-Rh alloy electrode interface using the phase-shift method. *Int. J. Hydrogen Energy* **2003**, *28*, 1333–1343.
(17) Chun, J. H. Methods for estimating adsorption isotherms in electrochemical systems *U.S. Patent* 2003, 6613218.
(18) Chun, J. H.; Jeon, S. K.; Kim, B. K.; Chun, J. Y. Determination of the Langmuir adsorption isotherms of under- and over-potentially deposited hydrogen for the cathodic H_2 evolution reaction at poly-Ir/aqueous electrolyte interfaces using the phase-shift method. *Int. J. Hydrogen Energy* **2005**, *30*, 247–259.
(19) Chun, J. H.; Jeon, S. K.; Ra, K. H.; Chun, J. Y. The phase-shift method for determining Langmuir adsorption isotherms of over-potentially deposited hydrogen for the cathodic H_2 evolution reaction at poly-Re/aqueous electrolyte interfaces. *Int. J. Hydrogen Energy* **2005**, *30*, 485–499.
(20) Chun, J. H.; Jeon, S. K.; Kim, N. Y.; Chun, J. Y. The phase-shift method for determining Langmuir and Temkin adsorption isotherms of over-potentially deposited hydrogen for the cathodic H_2 evolution reaction at the poly-Pt/H_2SO_4 aqueous electrolyte interface. *Int. J. Hydrogen Energy* **2005**, *30*, 1423–1436.
(21) Chun, J. H.; Kim, N. Y. The phase-shift method for determining adsorption isotherms of hydrogen in electrochemical systems. *Int. J. Hydrogen Energy* **2006**, *31*, 277–283.
(22) Chun, J. H.; Jeon, S. K.; Chun, J. Y. The phase-shift method and correlation constants for determining adsorption isotherms of hydrogen at a palladium electrode interface. *Int. J. Hydrogen Energy* **2007**, *32*, 1982–1990.
(23) Chun, J. H.; Kim, N. Y.; Chun, J. Y. Determination of adsorption isotherms of hydrogen and hydroxide at Pt-Ir alloy electrode interfaces using the phase-shift method and correlation constants. *Int. J. Hydrogen Energy* **2008**, *33*, 762–774.
(24) Chun, J. Y.; Chun, J. H. Correction and supplement to the determination of the optimum intermediate frequency for the phase-shift method [Chun et al., Int. J. Hydrogen Energy 30 (2005) 247−259, 1423−1436] *Int. J. Hydrogen Energy* **2008**, *33*, 4962−4965.
(25) Chun, J. Y.; Chun, J. H. A negative value of the interaction parameter for over-potentially deposited hydrogen at Pt, Ir, and Pt-Ir alloy electrode interfaces *Electrochem. Commun.* **2009**, *11*, 744−747.
(26) Kvastek, K.; Horvat-Radosevic, V. Comment on: Langmuir adsorption isotherms of over-potentially deposited hydrogen at poly-Au and Rh/H_2SO_4 aqueous electrolyte interfaces; Qualitative analysis using the phase-shift method, *J. Electrochem. Soc.* 150 (2003) E207−217. *J. Electrochem. Soc.* **2004**, *151*, L9–10.
(27) Lasia, A. Comments on: The phase-shift method for determining Langmuir adsorption isotherms of over-potentially deposited hydrogen for the cathodic H_2 evolution reaction at poly-Re/aqueous electrolyte interfaces, Int. J. Hydrogen Energy 30 (2005) 485−499. *Int. J. Hydrogen Energy* **2005**, *30*, 913−917.
(28) Chun, J. H.; Ra, K. H.; Kim, N. Y. Response to comment on: Langmuir adsorption isotherms of over-potentially deposited hydrogen at poly-Au and Rh/H_2SO_4 aqueous electrolyte interfaces; Qualitative analysis using the phase-shift method, J. Electrochem. Soc. 150 (2003) E207. *J. Electrochem. Soc.* **2004**, *151*, L11–13.
(29) Chun, J. H.; Jeon, S. K.; Kim, N. Y.; Chun, J. Y. Response to comments on: The phase-shift method for determining Langmuir adsorption isotherms of over-potentially deposited hydrogen for the cathodic H_2 evolution reaction at poly-Re/aqueous electrolyte interfaces, Int. J. Hydrogen Energy 30 (2005) 485−499. *Int. J. Hydrogen Energy* **2005**, *30*, 919–928.
(30) Gileadi, E.; Kirowa-Eisner, E.; Penciner, J. *Interfacial electrochemistry*; Addison-Wesley: Reading, MA, 1975; p 6, 72−73.
(31) Caprani, A.; Epelboin, I.; Morel, P. H. Potentiostatic investigation of the evolution of the cathodic current, near the corrosion potential, of a titanium rotating disc electrode in aerated sulphuric acid medium. *J. Less Common Metals* **1980**, *69*, 37–48.
(32) Gileadi, E.; Kirowa-Eisner, E.; Penciner, J. *Interfacial electrochemistry*; Addison-Wesley: Reading, MA, 1975; pp 86−93.
(33) Gileadi, E. *Electrode kinetics*; VCH: New York, 1993; pp 293−303, 428−443.
(34) Scully, J. R.; Silverman, D. C.; Kendig, M. W., Eds. *Electrochemical impedance: Analysis and interpretation*; ASTM: PA, 1993.
(35) Barsoukov, E.; Macdonald, J. R., Eds. *Impedance spectroscopy*, 2nd ed.; Wiley-Interscience: New York, 2005.
(36) Gileadi, E. *Electrode kinetics*; VCH: New York, 1993; pp 307−309.
(37) Gileadi, E. *Electrosorption: Adsorption in electrochemistry*; Gileadi, E., Ed.; Plenum Press: New York, 1967; pp 1−18.
(38) Gileadi, E. *Electrode kinetics*; VCH: New York, 1993; pp 261−280.
(39) Bockris, JO'M.; Reddy, A. K. N.; Gamboa-Aldeco, M. *Modern electrochemistry*, 2nd ed.; Kluwer Academic/Plenum Press: New York, 2000; pp 1193−1197; *Vol.* 2A.
(40) Bockris, JO'M.; Khan, S. U. M. *Surface electrochemistry*; Plenum Press: New York, 1993; pp 280−283.
(41) Gileadi, E.; Kirowa-Eisner, E.; Penciner, J. *Interfacial electrochemistry*; Addison-Wesley: Reading, MA, 1975; pp 82−86.
(42) Oxtoby, D. W.; Gillis, H. P.; Nachtrieb, N. H. *Principles of modern chemistry*, 5th ed.; Thomson Learning Inc.: New York, 2002; p 446.

Received for review August 12, 2008. Accepted February 1, 2009. This work was supported by the Research Grant of Kwangwoon University in 2009.

JE8006327